

PAPER

Synthesis and characterizations of alginate- α -tricalcium phosphate microparticle hybrid film with flexibility and high mechanical property as a biomaterial

To cite this article: Dipankar Das *et al* 2018 *Biomed. Mater.* **13** 025008

View the [article online](#) for updates and enhancements.

Recent citations

- [Bioactive Molecules Release and Cellular Responses of Alginate-Tricalcium Phosphate Particles Hybrid Gel](#)
Dipankar Das *et al*

Biomedical Materials



PAPER

Synthesis and characterizations of alginate- α -tricalcium phosphate microparticle hybrid film with flexibility and high mechanical property as a biomaterial

RECEIVED
2 May 2017

REVISED
25 September 2017

ACCEPTED FOR PUBLICATION
28 September 2017

PUBLISHED
24 January 2018

Dipankar Das^{1,2}, Shengmin Zhang³ and Insup Noh^{1,2}

¹ Department of Chemical and Biomolecular Engineering, Seoul National University of Science and Technology, Seoul 01811, Republic of Korea

² Convergence Institute of Biomedical Engineering and Biomaterials, Seoul National University of Science and Technology, Seoul 01811, Republic of Korea

³ Advanced Biomaterials and Tissue Engineering Center, Huazhong University of Science and Technology, Wuhan 430074, People's Republic of China

E-mail: insup@seoultech.ac.kr

Keywords: alginate, biomaterials, calcium phosphate, crosslinking, hybrid film

Abstract

A biocompatible hybrid film has been fabricated using alginate (Alg), α -tricalcium phosphate (α -TCP) microparticle and calcium chloride through ionic crosslinking as a biomaterial. The 'screeding method' (like a concrete finishing process) has been employed to develop the Alg- α -TCP film. For this method, the Alg/ α -TCP blend has been prepared using an ultra-sonicator and then put on a glass slide. After that, the excess volume of blend has been cut off by skidding another slide along with the surface of the blend to achieve proper grade and flatness. The mechanical strength and flexibility of the film (Alg- α -TCP) has been controlled by changing its compositions. The crosslinking phenomenon has been confirmed by attenuated total reflectance Fourier transform infrared spectroscopy (ATR-FTIR), ¹³C nuclear magnetic resonance (NMR), x-ray diffraction and thermogravimetric analyses. The ATR-FTIR and ¹³C NMR analysis results suggest that carboxylate groups of the alginate are ionically cross-linked with Ca²⁺ ions, while the α -TCP particles reside in the network by physical interaction. The micro-fatigue test results imply high tensile strength (up to 257 MPa) and flexibility (up to 13% elongation) of the Alg- α -TCP hybrid films. The SEM analysis suggests the α -TCP particles are homogeneously distributed on the surface of Alg- α -TCP films, whereas cross-sectional images confirmed the presence of α -TCP in the cross-linked network. TGA results demonstrated that thermal stability of the hybrid film was enhanced due to ionic crosslinking and interfacial interaction between alginate and α -TCP. The incorporation of α -TCP particles diminished the swelling ratio of the hybrid film. The *in vitro* bone cell (MC3T3) culture and cytotoxicity tests showed that the hybrid film is biocompatible. The hybrid film releases bovine serum albumin and dimethylxaloylglycine in a controlled way at pH 7 and 7.4, and 37 °C. Overall, the biocompatible Alg- α -TCP hybrid film with excellent mechanical strength and flexibility could be applied as an interfacial film in tissue engineering.

1. Introduction

For the past few years, interfacial tissue engineering gained noteworthy attention for repairing interface tissue defects. The regeneration of articular cartilage is always challenging since it has limited regenerative ability because of the absence of blood vessels, lymphatic vessels or neural tubes [1–3]. Based on the

depth of damage, cartilage defects are of three types: partial-thickness defects, full-thickness defects and osteochondral defects [1]. Osteochondral interface defects include injuries of both articular cartilage and underlying subchondral bone that are caused by trauma, disease, or aging [4, 5]. Fundamentally, osteochondral defects affect to the entire section of subchondral bone [1]. The subchondral bone shows a

vital role in providing support for the overlying articular cartilage [1]. Osteochondral defects without treatment may lead to progressive deterioration of cartilage, leading to osteoarthritis and finally, disabilities [1, 4, 5]. Consequently, it is essential to repair osteochondral defects to prevent osteoarthritis or disability.

The osteochondral interface is the border area of cartilage and subchondral bone. Different zones of cartilage (superficial, middle, deep, and calcified) consist of cells and extracellular matrix molecules (collagen) and exposed different amounts of stiffness [2]. The compressive modulus of subchondral bone (5.7 GPa) is higher than that of cartilage (0.079–320 MPa) [2]. The different compositions and mechanical strengths of bone and cartilage specify the intricacy of this tissue interface, creating interest for the development of tissue engineering materials [2]. Interfacial tissue engineering is an effective method to address the complexity of cartilage defects. Incidentally, the main criteria of the fabrication of biomimetic substances will be maintenance of similar biological and mechanical properties as observed in the native interface. In this aspect, biphasic scaffolds are superior to repair osteochondral defects because of the fabrication of adjusted microenvironments in different layers by altering the chemical, structural, and mechanical properties [1]. One phase was designed to repair cartilage tissue, and the other was intended to repair bone tissue. Furthermore, interface tissue engineering desires biocompatible and biodegradable porous substances for cell adhesion, proliferation and cell growth [2]. Numerous biomaterials and their derivatives such as alginate [6–9], chitosan [10–12], agarose [13, 14], hyaluronic acid [15, 16], gellan gum [17, 18], gelatin [12, 19, 20], collagen [20, 21], and fibroin [15, 22] were studied for reformation of deficient osteochondral interface or articular cartilage tissue because of their inherent biocompatibility, non-toxicity and biodegradability. Although natural materials can enhance biological interaction with host tissues, the low mechanical strength and instability of the materials compared to native cartilage sometimes create difficulties for its clinical applications [23]. On the other hand, bioactive ceramics such as hydroxyapatite, calcium phosphates, and silicate bioactive glasses are being extensively employed in bone tissue engineering because of their excellent osteoconductive/osteoinductive capabilities [2]. Consequently, osteochondral tissue engineering needs a single compound with a unique composition, association and adequate mechanical strength. Various alginate and calcium phosphate based hybrid scaffolds were developed for that purpose, such as alginate and α/β -tricalcium phosphate (TCP) based scaffolds which were designed for tissue engineering by 3D printer [24], a calcium phosphate cement–alginate porous scaffold that was fabricated for bovine serum albumin (BSA) and lysozyme delivery and bone tissue engineering [25], a

fibrous scaffold of calcium phosphate cement–alginate that was used for bone marrow stromal cell responses [26], core–shell type scaffolds of alginate/ α -tricalcium phosphate that was designed for cytochrome C protein delivery [27], and fabrication of core–shell fibrous scaffold that was carried out using cobalt chloride and calcium chloride for synergetic bone regeneration [28]. However, development of alginate/ α -TCP particle-based hybrid film with high mechanical strength and flexibility using the screeding method for the application of interfacial osteochondral defects is still not reported.

In the present study, a hybrid film (Alg- α -TCP) has been fabricated using alginate (Alg) as a biopolymer and α -TCP as a ceramic through ionic cross-linking by calcium chloride. Compared to other reported Alg/ α -TCP scaffolds, here a novel pathway, namely the ‘screeding method’ (like a concrete finishing process) has been applied to get better orientation of α -TCP micro-particles in the alginate matrix and to achieve flatness in film. The Alg/ α -TCP blend has been prepared by ultra-sonicator for the homogeneous distribution of the α -TCP particles so that the film can achieve sufficient stability and adequate mechanical properties. The fabricated Alg- α -TCP film showed good thermal stability. It also demonstrated high tensile strength (up to 257 MPa) and flexibility (up to 13% elongation). The *in vitro* bone cell (MC3T3) culture and cytotoxicity tests showed that the hybrid film is biocompatible. The hybrid film releases BSA and dimethylxaloylglycine (DMOG) in a controlled way at pH 7 and 7.4, and 37 °C. Finally, the Alg- α -TCP biocompatible film with high mechanical strength and flexibility could ideally promote the specific growth of both cartilage and subchondral bone by acting as an interfacial film in osteochondral defects.

2. Experimental

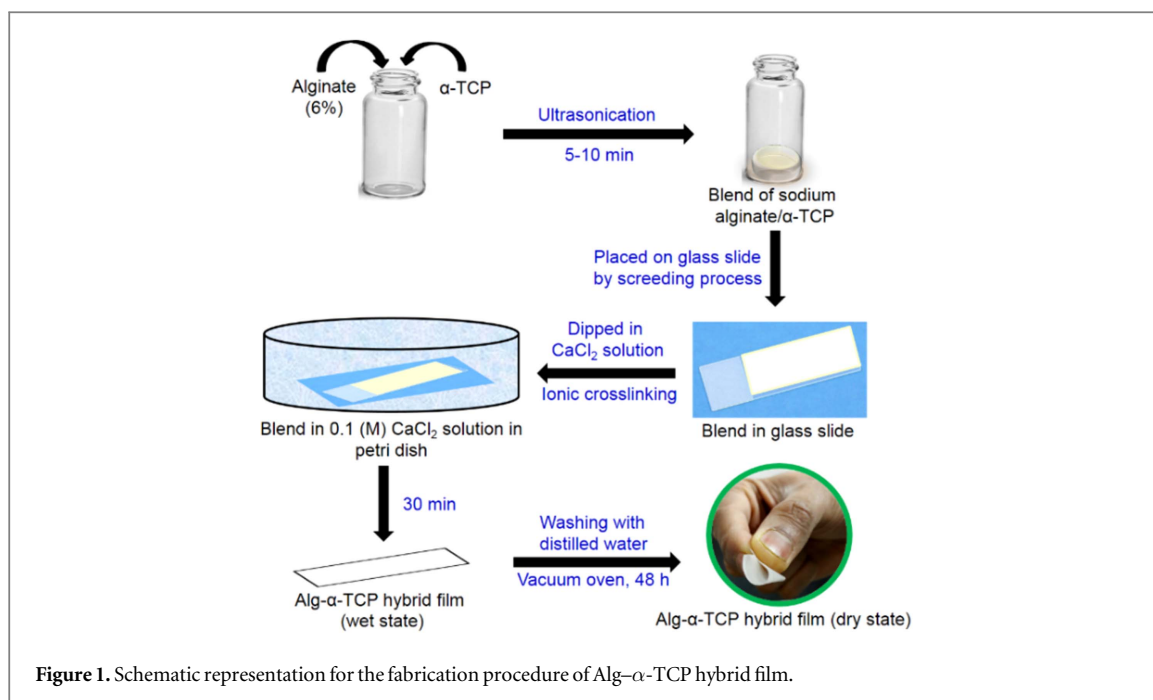
2.1. Chemicals

Alginic acid sodium salt (Alg, medium viscosity), calcium chloride (CaCl_2), calcium hydrogen phosphate dihydrate, BSA, and tetracycline (TCN) were purchased from Sigma Aldrich (USA). Double distilled water (DW) was employed for experimental purposes.

2.2. Synthesis

2.2.1. Synthesis of α -TCP by ball milling machine

The α -TCP micro-particles were synthesized by following the protocol reported by Woo *et al* [29]. In brief, calcium hydrogen phosphate dihydrate (68.84 g) was mixed with calcium carbonate (20.02 g) in a molar ratio of 2:1 and then 100 ml ethanol was added. The mixture was placed into a 500 ml alumina pot containing 100 g of zirconia particles of 5 mm diameter. Afterwards, the mixture was mixed with a ball milling machine (model: SBML-2, SciLab Korea Co.,



Ltd, Korea) at 150 rpm for 24 h. Then, the zirconia particles were retrieved using a sieve (diameter of pore = 425 μm ; Daehan Science, Korea). After that, the mixture of dicalcium phosphate and calcium carbonate was transferred to an aluminium tray and kept in heating oven at 70 $^{\circ}\text{C}$ for 24 h to remove ethanol. Then, the alumina pot containing the powder was heated up in an electrical furnace (model: MHS-160526-01, MiR furnace, Korea) at 1300 $^{\circ}\text{C}$ for 16 h using Segment-1 program (escalating of heating for 2 h and heating for 16 h and cooling by power off). After cooling, clusters of α -TCP particles were obtained. The α -TCP clumps were transferred into an engineering plastic pot containing a mixture of two kinds of zirconia particles ($d = 20 \text{ mm}$, 300 g and $d = 4 \text{ mm}$, 100 g) and 300 ml ethanol. The plastic pot was loaded in the ball milling machine and rotated at room temperature for 24 h. Finally, the dried α -TCP particles were collected by removing the ethanol at 70 $^{\circ}\text{C}$ in the heating oven. The dried α -TCP particles were characterized by Fourier transform infrared spectroscopy (FTIR), scanning electron microscopy (SEM), and x-ray diffraction (XRD) analyses and used for film fabrication.

2.2.2. Fabrication of hybrid film using alginate and α -TCP micro-particles through the screeding method

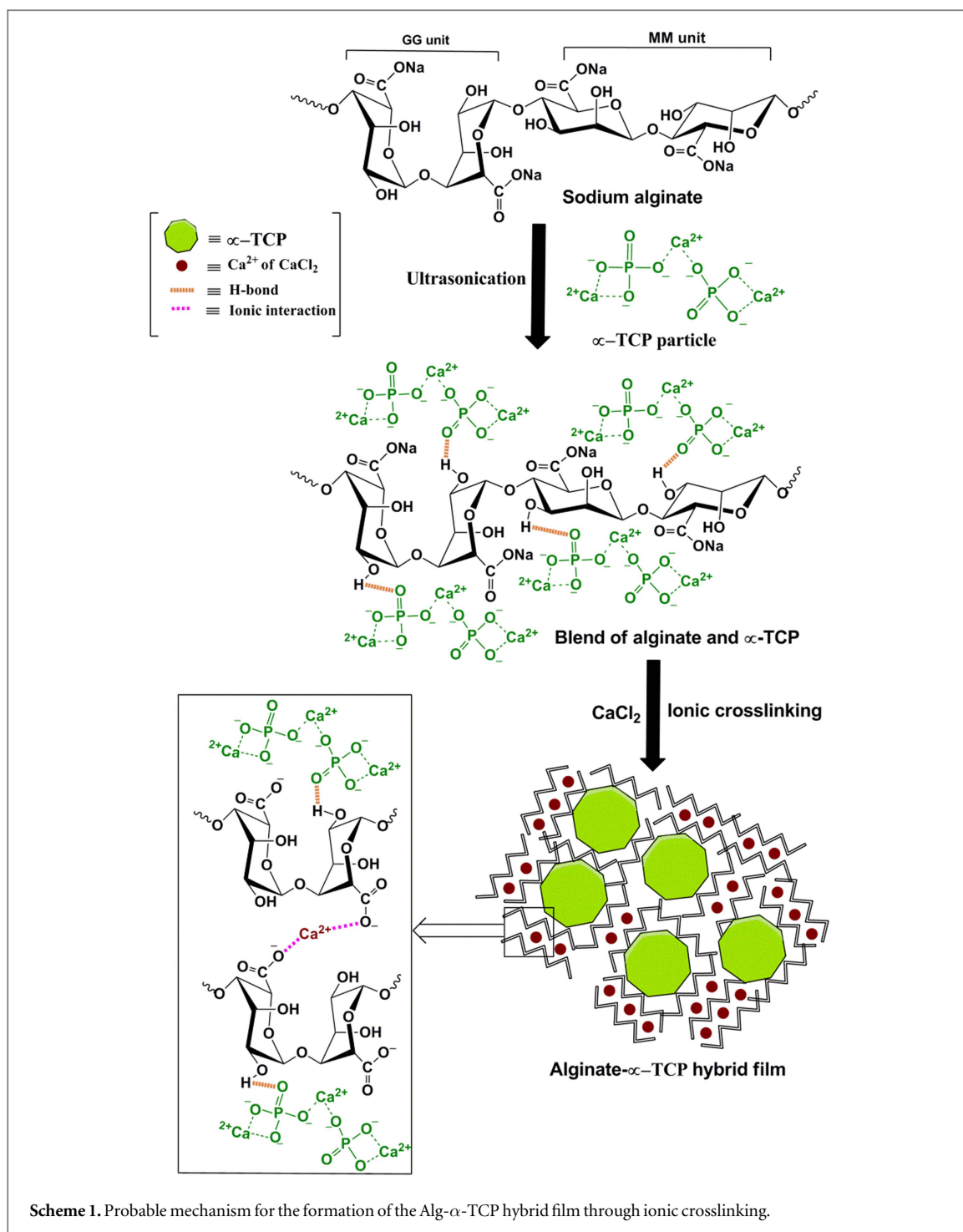
A hybrid film was prepared using alginate as biopolymer and α -TCP micro-particles as ceramics by ionic crosslinking. Briefly, sodium alginate (6 w/v %, 0.3 g) and required amounts of α -TCP (0.03, 0.15 and 3.0 g) were mixed in a 25 ml glass vial (figure 1).

After that, 5 ml double DW was added into the glass vial and a homogeneous blend was made using an ultra-sonicator (Sonics, Vibra Cell, South Korea) for 10 min. The film processing was performed by the

'screeding method' like a concrete finishing process. The prepared homogeneous blend was first placed on a glass slide (7.5 \times 2.5 cm^2). Then, the excess volume of blend was cut off through skidding another glass slide along with the surface of the blend to achieve proper grade and flatness. The screeding rate was $7.4 \pm 0.5 \text{ cm}^2 \text{ s}^{-1}$. Afterwards, the blend-loaded slide was immersed into 0.1 (M) CaCl_2 solution for 30 min for ionic crosslinking. The wet film (Alg- α -TCP) was washed three times with 100 ml DW. Finally, the film was dried in a vacuum oven at 40 $^{\circ}\text{C}$ for 48 h, until the steady weight was achieved.

For the Alg- α -TCP hybrid film, it is assumed that in presence of CaCl_2 , the carboxylate groups of alginate moiety cross-linked with Ca^{2+} ions. It is reported that alginate and divalent cations formed an egg-box like structure through ionic crosslinking [30–33]. The ultra-sonication process was used for the homogeneous distribution of the α -TCP micro-particles throughout the alginate network. Whereas, in contact with cross-linker (Ca^{2+}), alginate moieties linked with each other by cooperative mechanism [30]. Like an egg-box, cations (Ca^{2+}) can coordinate alginate chains by ionic interaction and form interconnected layers around the egg-box (scheme 1).

After ionic crosslinking, the network will squeeze its structure, where α -TCP micro-particles can orderly situated. Hence, the interfacial interaction between α -TCP micro-particles and alginate will be stronger, which may enhance the mechanical properties of the hybrid films. The ionic interaction between alginate and Ca^{2+} ions along with the probable interaction between α -TCP and alginate were examined by different chemical analyses and detailed explanation is described in section 3.



To observe the effect of amount of α -TCP micro-particles on the mechanical properties of the hybrid films, three different amounts of α -TCP (0.03 g, 0.15 g and 3.0 g) were mixed in 6% alginate solution (w/v%). The ratios (w/w) of alginate and α -TCP were 10:1, 2:1 and 1:10. The mechanical properties (tensile strength and flexibility) were evaluated by micro-fatigue tester (E3000LT, INSTRON, UK).

2.3. Characterizations

The FTIR spectra of alginate (sodium salt), α -TCP, dried Alg- α -TCP (10:1, 2:1 and 1:10) hybrid films, and dried Alg/ α -TCP (2:1) blend film without CaCl_2 were

recorded using an attenuated total reflectance (ATR)-FTIR spectrometer (model: Travel IR, Smiths Detection, USA) in powder state. The wavelength range was $650\text{--}4000\text{ cm}^{-1}$. The solid state ^{13}C nuclear magnetic resonance (NMR) analyses were executed with a NMR spectrometer (model: DD2 700, Agilent Technologies-Korea, USA). The XRD analyses of the samples were performed using an x-ray diffractometer (model: Bruker DE/D8 Advance, Bruker, USA). The thermogravimetric analysis (TGA) was carried out using a thermogravimetric analyzer (model: DTG-60, Shimadzu, Japan) under nitrogen atmosphere and the scan rate was $5\text{ }^\circ\text{C min}^{-1}$. The surface morphologies

of α -TCP, dried Alg- α -TCP hybrid films (10:1, 2:1 and 1:10), and Alg/ α -TCP (2:1) blend film without CaCl_2 were observed by SEM (model: SEM, TESCAN VEGA3, Tescan Korea). The cross-sections of the dried Alg- α -TCP hybrid films (10:1, 2:1 and 1:10) were investigated by field emission scanning electron microscope (FESEM, model: JSM-6700F, JEOL, Japan). The absorbance and % transmittance of the prepared Alg- α -TCP hybrid films (10:1, 2:1 and 1:10) were measured by a UV-visible (UV-vis) spectrophotometer (model: BioMATE 3, Thermo Scientific, USA).

2.4. Mechanical properties

The tensile strength and % elongation at break of the dried Alg- α -TCP hybrid films (10:1, 2:1 and 1:10) were measured at room temperature (25 °C) and 60%–65% relative humidity using a micro-fatigue tester (E3000LT, INSTRON, UK) followed by the ASTM protocol. The hybrid films were cut into strips ($5 \times 1 \text{ cm}^2$) and settled between the grips of the apparatus. The distance between the grips and gage length of the sample films were 15 mm and 20 mm, respectively. The crosshead speed was 1 mm s^{-1} .

2.5. Swelling study

The % swelling of the fabricated hybrid films were measured gravimetrically. In brief, the pre-weighed, dried hybrid films ($4 \times 2 \text{ cm}^2$) were immersed in 50 ml DW at 25 °C for 24 h. After a regular time interval (1 h), the hybrid films were taken out from DW, the surface water was blotted off by tissue paper and then reweighed. The experiment was carried out until the equilibrium weights of the films were reached. The % swelling was calculated by equation (1):

$$\text{Swelling (\%)} = \frac{\text{Final weight of the film} - \text{Initial weight of the film}}{\text{Initial weight of the film}} \times 100(\%). \quad (1)$$

2.6. Determination of opacity and light transmittance of the hybrid films

The opacity and UV light transmittance of the Alg- α -TCP hybrid films were evaluated by measuring absorbance and % transmittance by UV-vis spectrophotometer [34]. Briefly, the fabricated hybrid films (thickness $20 \pm 5 \mu\text{m}$) were cut into a rectangular shape ($2 \times 1 \text{ cm}^2$). The scanning of the hybrid films was performed with air as reference between 200–800 nm. The opacity of the hybrid films was calculated using equation (2):

$$\text{Opacity(\%)} = \frac{\text{Absorbance at 600 nm}}{\text{Thickness of the hybrid film}} \times 100(\%). \quad (2)$$

2.7. In vitro cytocompatibility study using MC3T3 cell line

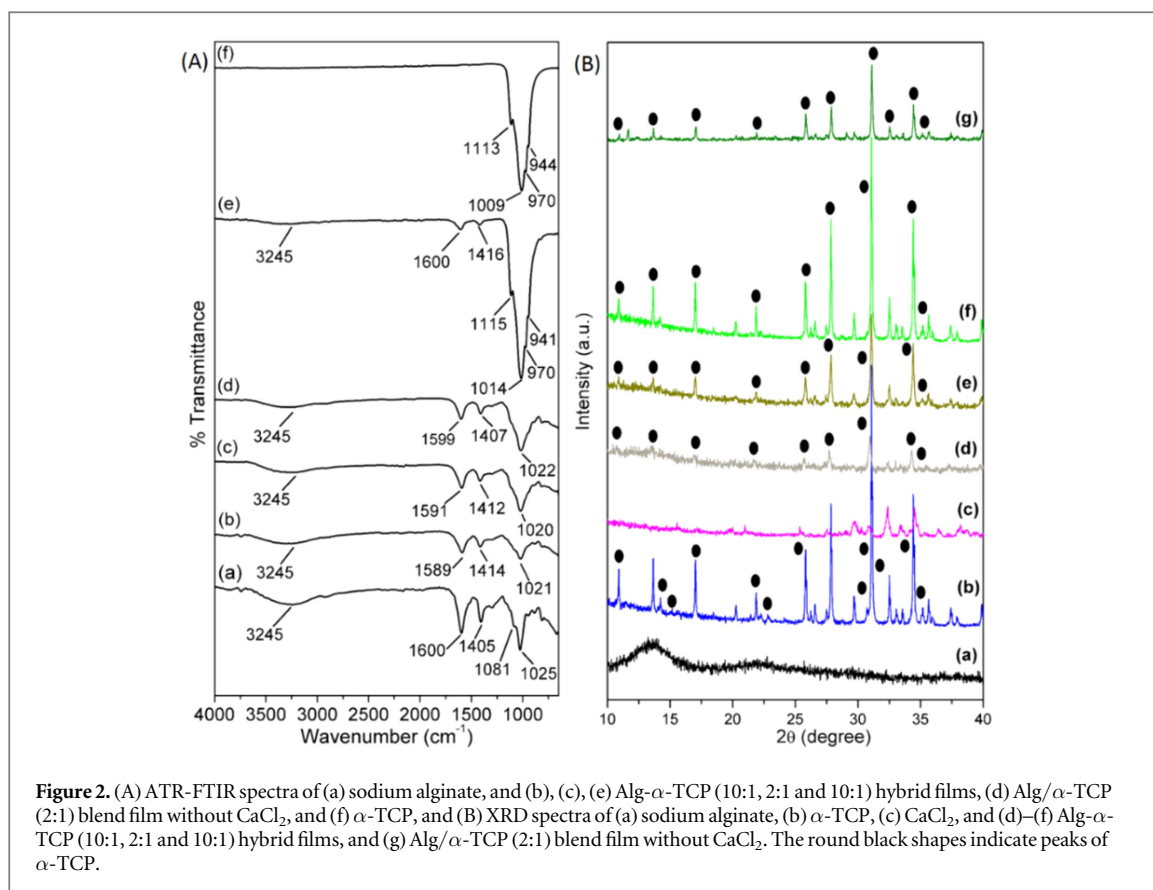
2.7.1. Cell proliferation on the surface of Alg- α -TCP (2:1) hybrid film

An osteoblast cell line derived from *Mus musculus* (mouse) calvaria (MC3T3-E1 cell line, Sigma Aldrich) were cultured in a 24-well plate. α -minimum essential media (MEM) (Sigma Aldrich, USA) containing 10% fetal bovine serum (Gibco Korea, Korea) and penicillin–streptomycin (100 unit ml^{-1}) was added to each well and then incubated for 24 h with 5% CO_2 at 37 °C. Teflon, latex and Alg- α -TCP (2:1) hybrid films ($0.8 \times 0.8 \text{ cm}^2$) were sterilized by autoclave (AC-02, Jeio Tech; Seoul, Korea). Then, $30 \mu\text{l}$ of media containing $2 \times 10^5 \text{ cells ml}^{-1}$ of MC3T3 cells were poured on the surface of each film in a 24-well plate by 1 ml syringe. The cells containing films were incubated for 4 h and then reverse those. Subsequently, α -MEM was supplied to each well and changed after every 24 h. The cells culture study was performed up to 7 days.

Live and dead assay for MC3T3 cells were carried out according to the protocol of the vendor (Invitrogen, USA). Briefly, a 9:1 mixture of α -MEM and CCK-8 solution (Dojindo Lab., Kumamoto, Japan) (9:1) was prepared. Then, 1 ml mixture solution was added to each well after removing the old media and incubated for 2 h. After that, the solution was transferred to another empty plate, 1 ml of 10% FBS medium was added to wells and incubated for 10 min. Then, $100 \mu\text{l}$ of solution was taken into 96 wells plate and absorbance was measured at a wavelength of 450 nm. The images of the live and dead cells were taken after the addition of $1.2 \mu\text{l}$ of 2 mM ethidium homodimer-1 (EthD-1) and $0.3 \mu\text{l}$ of 4 mM calcein AM into $600 \mu\text{l}$ phosphate-buffered saline. After addition of the two agents to each well followed by removing the media, the plate was incubated for 30 min. The cell images were captured by fluorescence microscope (Leica DMLB, Germany).

2.7.2. Cell behavior in presence of the extract solution of Alg- α -TCP (2:1) hybrid film

The extract solutions of Teflon, Latex and Alg- α -TCP (2:1) hybrid film ($0.8 \times 0.8 \text{ cm}^2$) were prepared by immersing three films into α -MEM containing 10% fetal bovine serum (Gibco Korea, Korea) and penicillin–streptomycin (100 unit ml^{-1}) in a 24-well plate for 72 h incubation. On the other hand, 2×10^5 no. of MC3T3 cells were seeded and cultured into α -MEM containing 10% fetal bovine serum (Gibco Korea, Korea) and penicillin–streptomycin (100 unit ml^{-1}) in a 24-well plate in a 96-well plate. Then, it was incubated in an incubator with 5% CO_2 atmosphere at 37 °C for 24 h. Afterwards, the media was removed and $100 \mu\text{l}$ of each extract was added into each cell well and cultured for another 24 h. Teflon and Latex were used as positive and negative controls, respectively. The live and dead cells images were captured using



ethidium homodimer-1 (EthD-1) and calcein AM solutions followed by same protocol as above. The cell images were captured by fluorescence microscope (Leica DMLB, Germany).

2.8. In vitro protein and drug release study

2.8.1. Preparation of bovine albumin serum (BSA) and dimethyloxallyl glycine (DMOG) incorporated Alg- α -TCP (2:1) hybrid film

BSA as a model protein and DMOG as a model antibiotic drug (5×10^{-6} mol) were incorporated into the hybrid film by mixing BSA and DMOG separately during blend preparation. After that, the hybrid film was made by the screeding process and then dried in an oven for 48 h. Afterwards, BSA and DMOG incorporated hybrid films were cut into round ($d = 10$ mm and width = $25 \mu\text{m}$) films. Each film contained 0.5×10^{-6} mol of drug and protein. These films were employed for release experiment.

2.8.2. In vitro release study

The *in vitro* release study of BSA and DMOG incorporated hybrid films were carried out at two pHs (7.0, 7.4) and human body temperature (37°C). The amount of BSA, and DMOG release were measured spectrophotometrically using UV-vis spectrophotometer (BioMate 3 s, Thermo Scientific). Briefly, dried BSA, and DMOG incorporated hybrid films were put into 10 ml buffer solutions in the 25 ml screw Teflon bottles (Daihan Scientific, Korea). After predefined

intervals (1, 3, 6, 24, 48, 72, 96, 120, 144 and 168 h), solutions were taken out from the Teflon bottles and spectra were recorded. After each measurement, the solutions were returned back to the bottles.

3. Results and discussions

3.1. Characterization

Figure 2 represents the ATR-FTIR spectra of sodium alginate, the dried Alg- α -TCP (10:1, 2:1 and 1:10) hybrid films, α -TCP particle and Alg/ α -TCP (2:1) blend film without CaCl₂. In the FTIR spectrum of sodium alginate (figure 2(A-a)), the peaks at 3245, 1600, and 1405 cm^{-1} are due to stretching vibrations of O-H bond and carboxylate groups (C=O, C-O), respectively. The peaks at 1081 and 1025 cm^{-1} are responsible for the asymmetric and symmetric stretching vibrations of C-O bond of polysaccharide ring, respectively. In the spectrum of α -TCP (figure 2(A-f)), the peaks at 1113, 1009, 970 and 944 cm^{-1} are because of the asymmetric and symmetric stretching vibrations of P-O bonds, respectively. From the FTIR spectrum of the dried Alg- α -TCP (1:10, 2:1 and 1:10) hybrid films (figure 3(A-b, c, e)), it is observed that the peak intensity of carboxylate groups (1600 and 1405 cm^{-1}) decreased sharply. While, the decreasing trends of peak value of C=O group was also noticed. This phenomenon indicates the ionic crosslinking reaction between the carboxylate groups of alginate and Ca²⁺ ions (scheme 1). Whereas in the FTIR

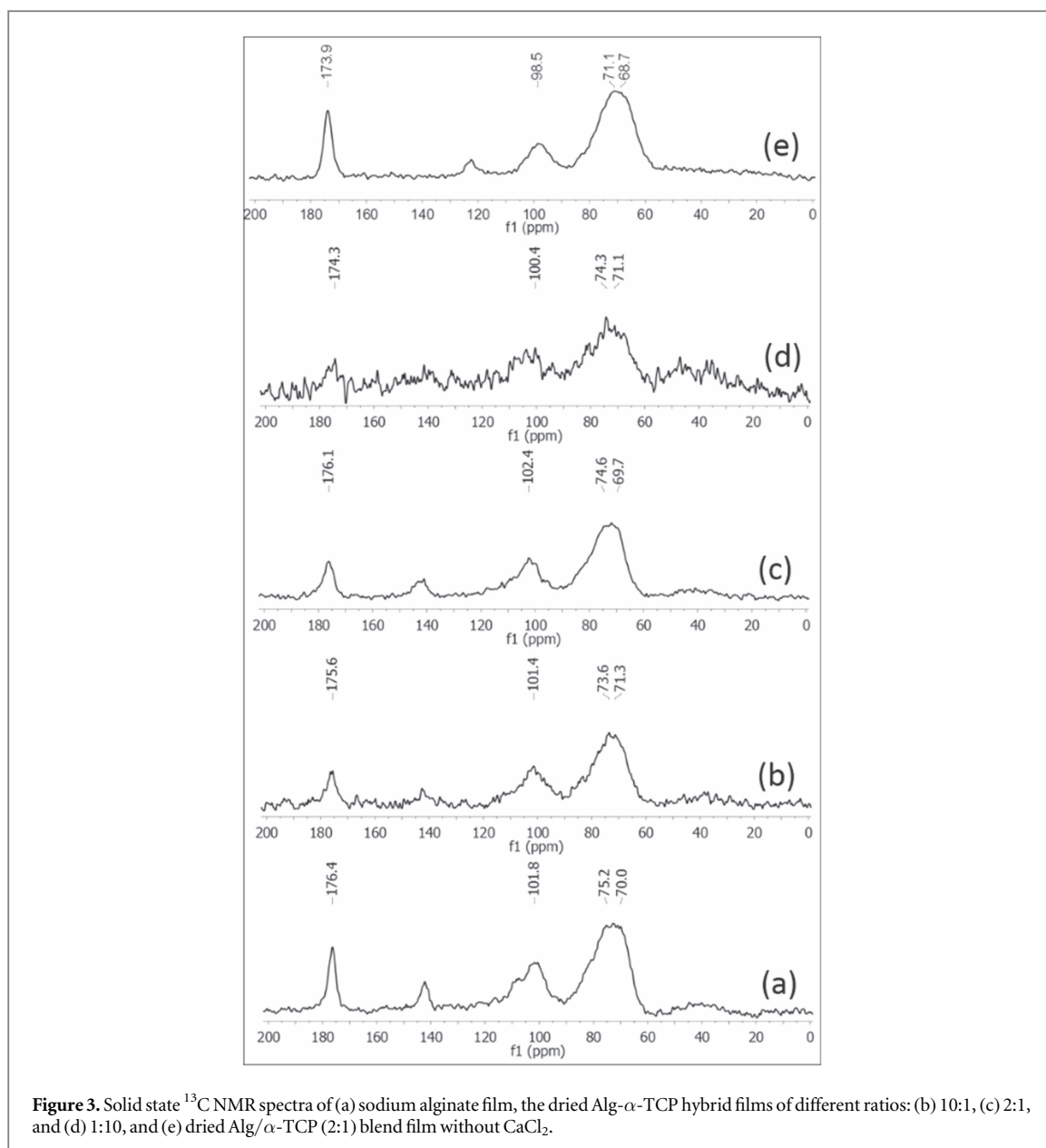


Figure 3. Solid state ^{13}C NMR spectra of (a) sodium alginate film, the dried Alg- α -TCP hybrid films of different ratios: (b) 10:1, (c) 2:1, and (d) 1:10, and (e) dried Alg/ α -TCP (2:1) blend film without CaCl_2 .

spectrum of Alg/ α -TCP (2:1) blend film (figure 2(A-d)) without CaCl_2 , no difference of C=O stretching frequency was found, which suggests that the presence of CaCl_2 is responsible for ionic crosslinking in the gel network. Besides, the progressive broadness of O-H stretching vibration (3245 cm^{-1}) clearly implies that the physical interaction (H-bonding) exists between α -TCP micro-particles and alginate.

In XRD analysis, sodium alginate (figure 2(B-a)) showed a broad peak at $2\theta = 13.7^\circ$, which implies the amorphous nature of alginate. The α -TCP particles demonstrated peaks at $2\theta = 10.9^\circ, 14.2^\circ, 15.1^\circ, 17^\circ, 21.9^\circ, 22.2^\circ, 22.7^\circ, 24.1^\circ, 30.7^\circ, 31^\circ, 31.1^\circ, 34.5^\circ, 35.1^\circ$ (figure 2(B-b)), which indicate crystalline state of α -TCP [35, 36]. While, CaCl_2 demonstrated peaks at $2\theta = 29.4^\circ, 32.3^\circ, 33.3^\circ, 34.4^\circ, 36.5^\circ$ and 38.1° (figure 2(B-c)), those are because of the crystalline nature of CaCl_2 . In the XRD spectra of the dried Alg- α -TCP hybrid films with and without CaCl_2 (figure 3(B-d-g)), it

has been observed with the increase of α -TCP amount, the peak of alginate moiety was suppressed. This phenomenon indicates that the amorphous nature of alginate is diminished by the accumulation of α -TCP particles and a physical interaction exists between alginate and α -TCP. Besides, it is also obvious from the figure 3(B-d-f) that with increase of the amount of α -TCP, the intensity of the characteristic peaks of α -TCP increased. This behavior confirms that the crystallinity of α -TCP remained intact in the ionically cross-linked network, which may affect the mechanical properties of the hybrid films.

In the solid state ^{13}C NMR spectrum, sodium alginate (figure 3(a)) demonstrated four chemical shifts at 70.0, 75.2, 101.8 and 176.4 ppm, which are responsible for the ring carbons of polysaccharide, anomeric carbon and carbonyl carbon of carboxylate group, respectively. While in the NMR spectra of the dried Alg- α -TCP (10:1, 2:1 and 1:10) hybrid films

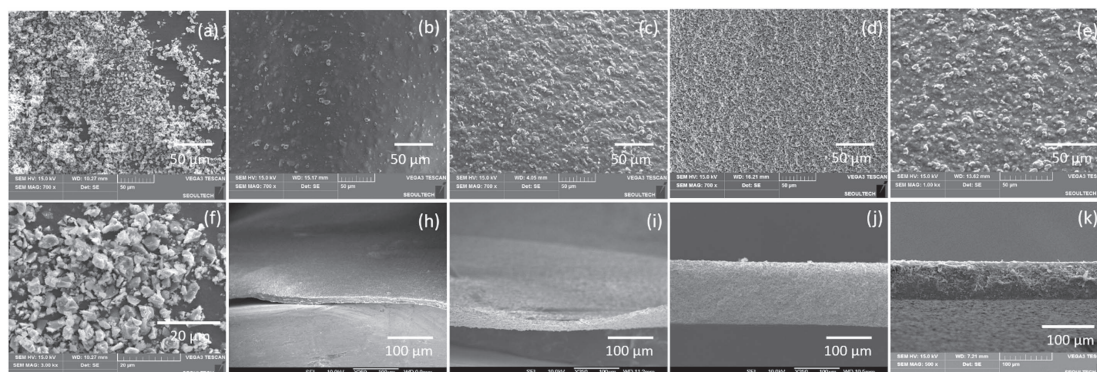


Figure 4. Surface morphologies of (a), (f) α -TCP, (b), (c), (d) Alg- α -TCP hybrid films (b) 10:1, (c) 2:1, and (d) 1:10, (e) Alg/ α -TCP (2:1) blend film without CaCl_2 analyzed by SEM, and cross-section images of the Alg- α -TCP hybrid films (h) 10:1, (i) 2:1, and (j) 1:10, analyzed by FESEM, and (k) cross-section image of Alg/ α -TCP (2:1) blend film without CaCl_2 analyzed by SEM.

(figures 3(b)–(d)), the intensities of the chemical shifts for carbonyl carbons of carboxylate group decreased and the peaks became relatively broadened, which may be because of the ionic crosslinking between carboxylate ions and Ca^{2+} ions. Furthermore, the NMR spectrum of the dried Alg/ α -TCP (2:1) blend film without CaCl_2 showed a sharp chemical shift for the carbonyl carbon of the carboxylate group at 173.9 ppm (figure 3(e)). This result confirmed that the broadness of the chemical shift for the carbonyl carbon of the carboxylate group happened due to the ionic crosslinking between carboxylate ion and Ca^{2+} ion.

Figure 4 describes the surface morphologies of α -TCP, the dried Alg- α -TCP (10:1, 2:1, and 1:10) hybrid films, and Alg/ α -TCP (2:1) blend film without CaCl_2 . From the figures 4(a) and (f), it is observed that α -TCP clearly appeared as micro-level particles with uneven shapes. The particle size ranges are between 0.5 and 8 μm . After fabrication, the hybrid films appeared with a rough surface (figures 4(b)–(e)), where α -TCP particles are embedded into the alginate network. In the case of the 1:10 hybrid film (figure 4(d)), α -TCP particles agglomerated in the surface of the film which increased the roughness of the surface. The distribution of α -TCP particles was comparatively homogeneous in 10:1 and 2:1 film (figures 4(b) and (c)). Owing to the incorporation of α -TCP particles into the cross-linked network, penetration of water molecules into the film would be difficult, which may affect the swelling property of the films. From the cross-section images (figures 4(h)–(k)), it is observed that α -TCP particles are not only present on the surface of the films, but also present into the interior of the cross-linked network. The thickness of the Alg- α -TCP films were approximately 15–20 μm . The presence of a large number of relatively bigger α -TCP particles were observed on the surface of Alg/ α -TCP blend film (without CaCl_2 , figure 4(e)) compared to the film with CaCl_2 .

In the TGA graph of sodium alginate (figure 5(a)), three zones of weight loss are apparent. The first weight loss zone (26 $^{\circ}\text{C}$ –100 $^{\circ}\text{C}$) is because of the presence of moisture, the second one (186 $^{\circ}\text{C}$ –377 $^{\circ}\text{C}$) is due to breakdown of the alginate chain and the third zone (550 $^{\circ}\text{C}$ –625 $^{\circ}\text{C}$) is from the evaporation of CO_2 . In the TGA plots, the Alg- α -TCP hybrid films (figure 5(a)) demonstrated three weight loss regions. The first zone (26 $^{\circ}\text{C}$ –100 $^{\circ}\text{C}$) is owing to the existence of moisture, the second zone (182 $^{\circ}\text{C}$ –407 $^{\circ}\text{C}$) is for the breakdown of alginate backbone and the third zone (462 $^{\circ}\text{C}$ –525 $^{\circ}\text{C}$) is due to the evaporation of CO_2 . The second zone is very crucial to determine the thermal stability of the hybrid film [34]. It was also observed that ~42%, 35%, 30% and 7% weight loss occurred in the second zone for alginate and the hybrid films (10:1, 2:1 and 1:10), respectively. For the Alg/ α -TCP (2:1) blend film without CaCl_2 , it was 34% (figure 5(a)). The residual weights are found to be 20.9%, 25.9%, 44.9% and 91.4% for alginate, and the hybrid films (10:1, 2:1 and 1:10), respectively.

The residual weight of Alg/ α -TCP (2:1) blend film without CaCl_2 is 40.1% (figure 5(a)). Hence, the nature of TGA curves reflect that the thermal stability of the hybrid films is enhanced because of both the ionic crosslinking and incorporation of α -TCP micro-particles. The Alg/ α -TCP (2:1) blend film without CaCl_2 showed a higher % residual weight (40.1%) compared to alginate (20.9%). This result confirmed that the interfacial interaction (mainly physical interaction: H-bonding) between alginate and ceramics (α -TCP) also affected on the thermal stability of the films and thus weight loss was lower for Alg/ α -TCP (2:1) blend film than that of native alginate film. Because of the thermal stability of the prepared film, it can be potentially used in antibacterial and antifungal coatings, food packaging, and biomedical devices [37].

3.2. Mechanical properties

Figure 5(b) and table 1 depict the tensile strength and % elongation at break of the hybrid films. It has

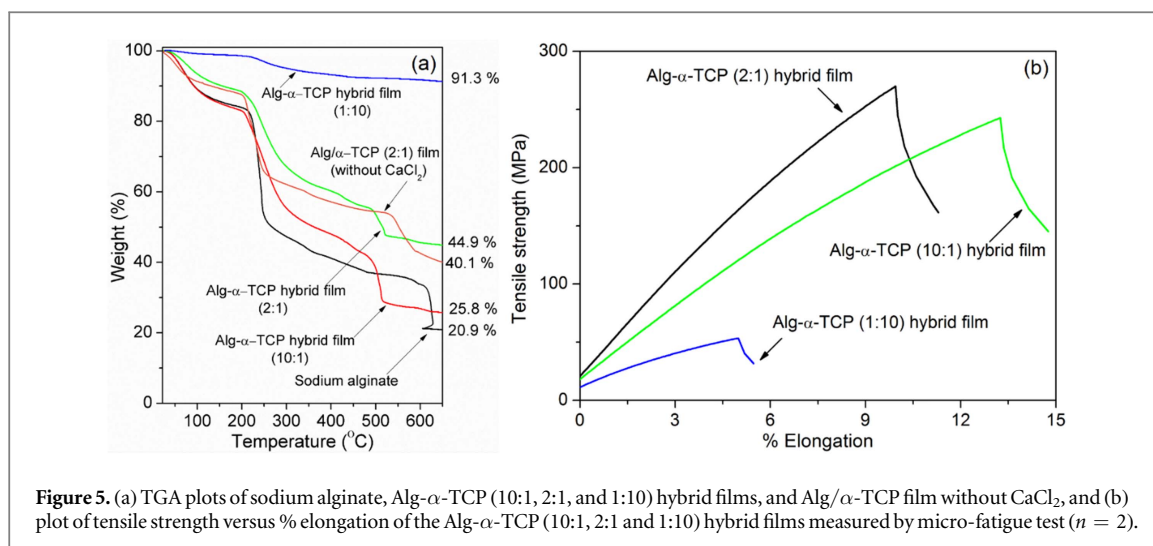


Table 1. Thickness, % elongation and tensile strength of the Alg- α -TCP (10:1, 2:1 and 1:10) hybrid films (results are average values, $n = 2$).

Hybrid films (Alg: α -TCP)	Thickness (μm)	Elongation (%)	Tensile strength (MPa)
10:1	20 \pm 5	13.23	254.51
2:1	20 \pm 5	10.50	257.52
1:10	20 \pm 5	4.44	38.48

been observed that % elongation of the hybrid films decreased with addition of α -TCP micro-particles.

The higher tensile strength of the hybrid film depends on both the distribution of α -TCP as filler into the alginate network as well as the interaction between α -TCP and alginate. From table 1, it is obvious that the tensile strength of the 2:1 (Alg : α -TCP) hybrid film is highest among three hybrid films. This is owing to the fact that a comparatively homogeneous distribution of α -TCP micro-particles was seen in the 2:1 hybrid film (figure 4(c)), resulting in a stronger interfacial interaction which may have formed between α -TCP and alginate. The interfacial interaction in 10:1 hybrid film will be the smallest because of the presence of the lowest amount of α -TCP micro-particles. In the case of the 1:10 hybrid film, a large amount of α -TCP micro-particles make for an irregular distribution and agglomeration, which hindered the effect of α -TCP micro-particles towards the mechanical properties.

3.3. Swelling study

Figure 6 describes % swelling of the Alg- α -TCP hybrid films at pH 7, 7.4 and 37 °C. The hybrid films reached their equilibrium swelling state at \sim 10 h. It has been detected that % swelling of 10:1 Alg- α -TCP hybrid film is higher, and lower for 1:10 Alg- α -TCP hybrid film in both media. This phenomenon can be explained by the fact that swelling of the Alg- α -TCP hybrid film depends on the presence of functional

hydrophilic groups, availability of hydrophilic groups, crosslinking density and distribution of the filler (α -TCP particles) into the film network. For Alg- α -TCP (10:1) film, the availability of hydrophilic groups is highest due to presence of higher % alginate moiety. Thus, it can absorb a large volume of water, resulting in higher % swelling. While in 1:10 film, due to the existence of lowest % alginate moiety, the lowest % swelling was observed. Again, from the FTIR spectra (figure 2(A-b, c, e)), it has been observed that the hydroxyl groups of the alginate moiety are connected by physical interactions with α -TCP particles. Thus, the availability of hydroxyl groups will be highest where % alginate is highest (10:1). Furthermore, because of the presence of the lowest amount of α -TCP, the density of α -TCP particles in the 10:1 hybrid film network will be less compared to 2:1 and 10:1 hybrid films. For this reason, the void space in the cross-linked network will be highest in the case of the 10:1 hybrid film, while it will be lowest for the 1:10 hybrid one. Hence, the order of % swelling of Alg- α -TCP hybrid films is 10:1 > 2:1 > 1:10. From figure 7, it is also obvious that % swelling is higher at basic media (pH 7.4) compared to neutral media (pH 7). The results may be owing to the fact that, at pH 7.4, the crosslinking agent (Ca^{2+}) may have formed new compounds with the ions present in buffer media. Thus, the crosslinking network may be broken, which increased the space for water diffusion into the hybrid gel network, resulting in higher % swelling. At pH 7, the polymer network remained intact, therefore absorbed fewer water molecules and showed lower % swelling than that at pH 7.4.

3.4. Determination of opacity and light transmittance of the hybrid films

The aim of this study was to observe the effect of distribution patterns of α -TCP particles in the alginate network towards the light transmittance property. The opacity and light transmittance properties of the Alg- α -TCP (10:1, 2:1, 1:10) hybrid films have been

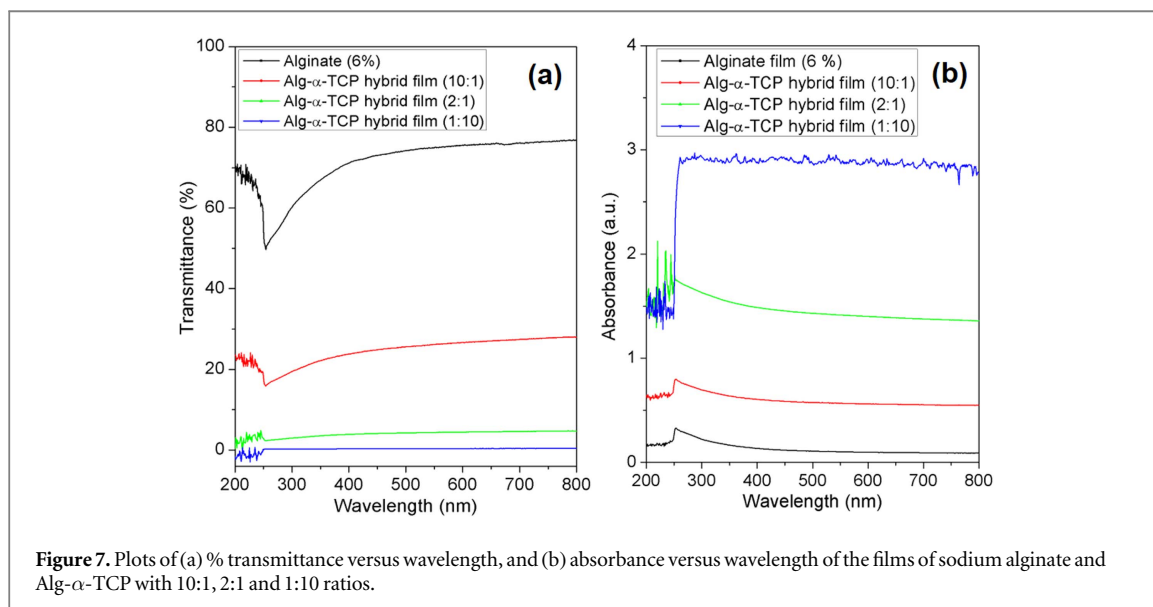
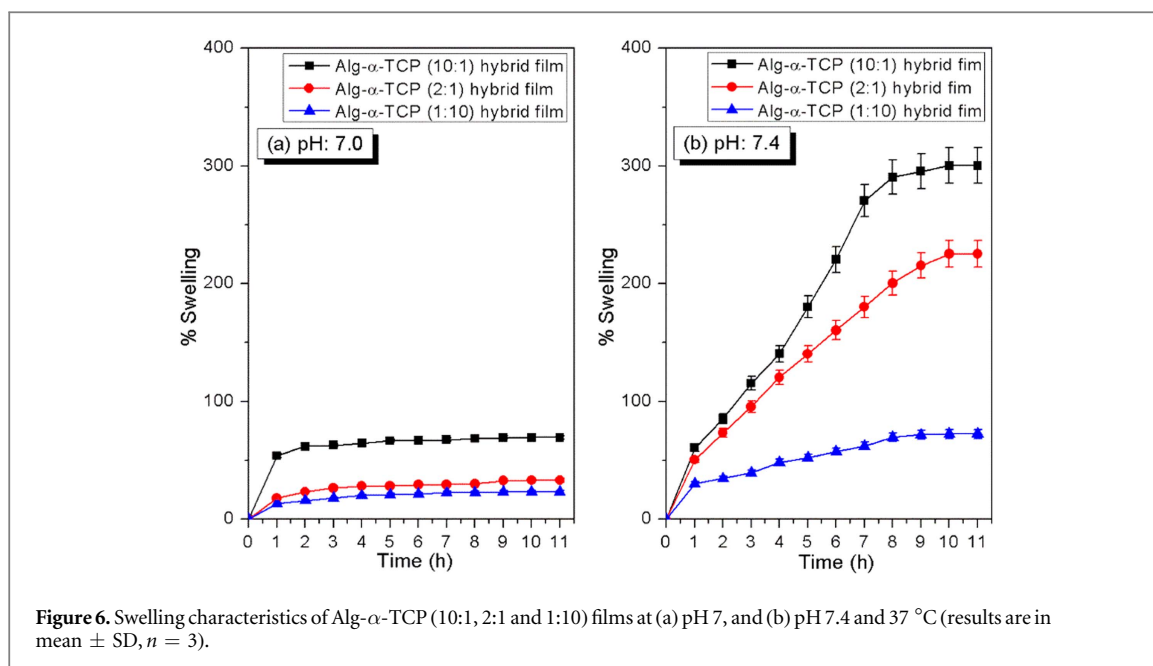


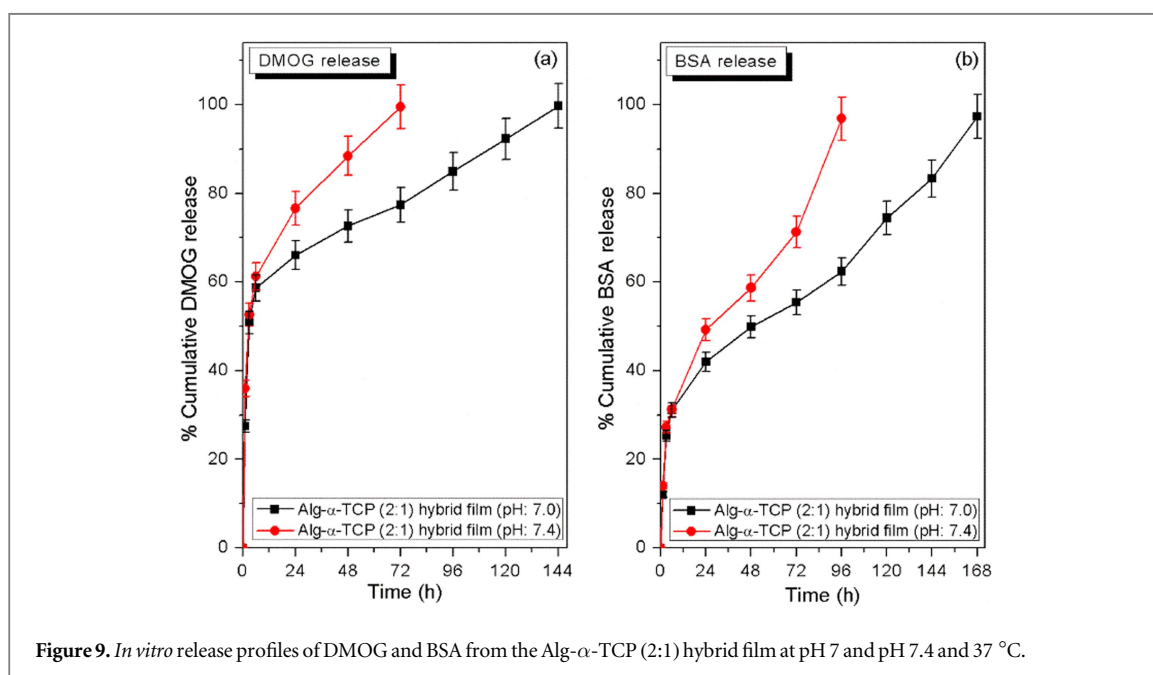
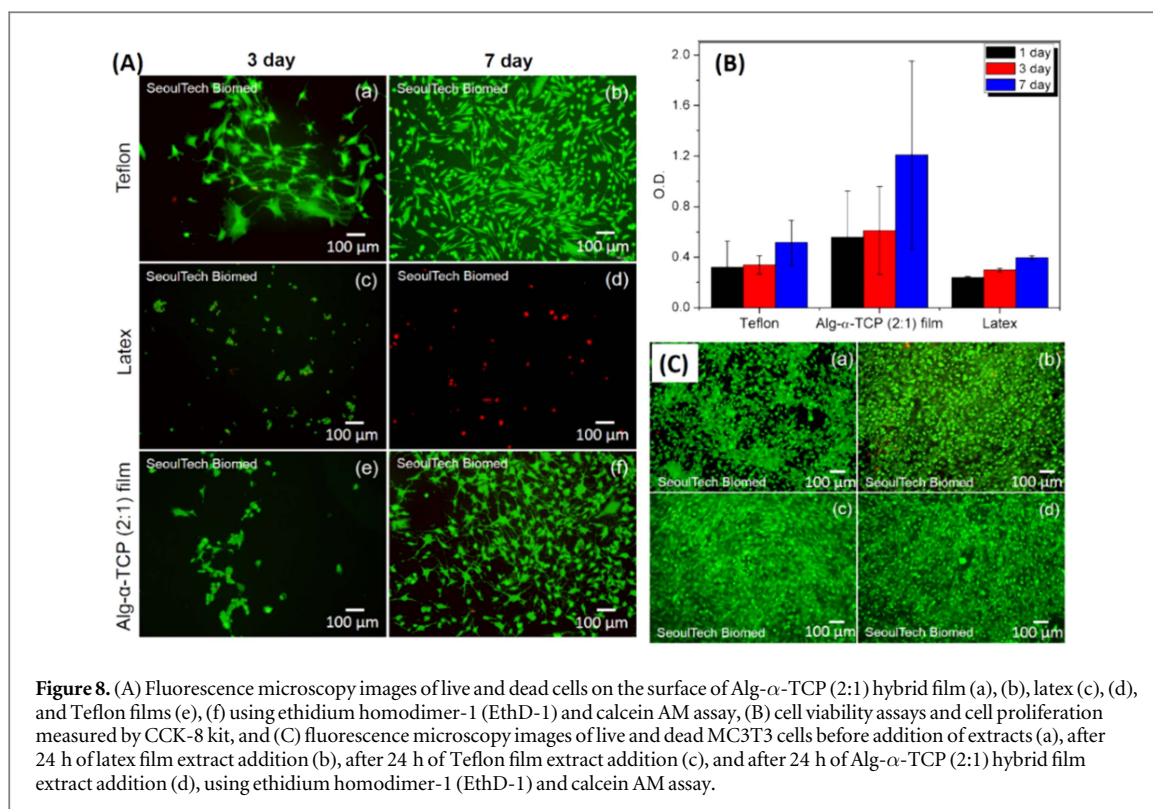
Table 2. Opacity and % transmittance values of alginate and Alg- α -TCP hybrid films (results in mean \pm SD, $n = 3$).

Films	Thickness (μm)	Opacity (mean \pm SD)	% Transmittance (mean \pm SD)
6% alginate	20 \pm 5	1.96 \pm 0.12	48.58 \pm 0.73
Alg- α -TCP (10:1)	20 \pm 5	6.61 \pm 0.27	16.72 \pm 0.59
Alg- α -TCP (2:1)	20 \pm 5	14.01 \pm 0.33	2.23 \pm 0.06
Alg- α -TCP (1:10)	20 \pm 5	28.90 \pm 1.72	0.40 \pm 0.11

evaluated on the basis of the maximum wavelength at 600 nm by UV-vis spectrophotometer.

It is observed that the alginate film showed lower opacity than those of hybrid films, which indicates a high transparency of the alginate film (table 2). As concentrations of α -TCP micro-particles are increased, the opacity of the hybrid films increases (α -TCP). It has also been noticed that the alginate film demonstrated the highest value of % transmittance of UV

light (48.58% at 254 nm). Whereas in the case of hybrid films, the increase of α -TCP micro-particles amounts decreased the % transmittance values i.e., 16.72% and 0.04% for 10:1 and 1:10, the hybrid films, respectively (figure 8(a) and table 2). These results indicate that the incorporation of α -TCP micro-particles deterred the photo-permeability through the hybrid films. The decrease of film transparency is because of the homogenous distribution of ceramic



particles (α -TCP) in the cross-linked network as well as the good interfacial interaction between alginate and α -TCP [38]. The large decrease of film transparency in high α -TCP content implies the existence of the agglomeration and self-networking of α -TCP within the alginate matrix which hinders light passage through the alginate film [38]. The lower transmission of UV light between 200 and 250 nm indicates that the Alg- α -TCP film could prevent damage to lipids and medical devices from UV light [34].

3.5. *In vitro* cytocompatibility study

Figure 8 shows *in vitro* cell study results of Alg- α -TCP (2:1) hybrid film using MC3T3 cells line up to 7 days. From figures 8(A) and (B), it is obvious that compared to Teflon (figure 8(A-a, b)) and latex (figure 8(A-c, d)) film, the number of cells on the surface of Alg- α -TCP hybrid film (figure 8(A-e, f)) increases with the progress of time from 1 day to 7 days. It is also apparent that all cells were dead at day 7 on latex (figure 8(A-d)), whereas no dead cells were found in Teflon and hybrid films (figure 8(A-b

and f)). The results imply that the surface of Alg- α -TCP (2:1) hybrid film showed excellent cell viability and cell proliferation and thus the hybrid film is biocompatible. Figure 8(C) demonstrates the effect of extracts from Alg- α -TCP (2:1) hybrid film, latex and Teflon films on MC3T3 cells after 24 h. It is observed that all cells are alive and grown in the extract solutions of Teflon and Alg- α -TCP (2:1) hybrid films (figure 8(C-c, d)), while the extract of latex induced some cell death (figure 8(C-b)). The results indicate the nontoxic nature of the Alg- α -TCP (2:1) hybrid film.

3.6. *In vitro* release of DMOG and BSA from Alg- α -TCP (2:1) hybrid film

Figure 9 depicts the *in vitro* release profiles of an antibiotic drug (DMOG) and protein (BSA) from the Alg- α -TCP (2:1) hybrid film at 37 °C. The Alg- α -TCP hybrid film (2:1) has been selected for the release study because of its good flexibility and higher mechanical strength (table 2). From figure 9, it is apparent that the shapes of release curves are different which are associated with the higher release rate of DMOG in both media (pH 7 and 7.4) compared to BSA (figures 9(a) and (b)). Due to the lower molecular weight (175.1 g mol⁻¹) and smaller particle size of DMOG than that of BSA (~66 kDa), the solubility and mobility of DMOG in aqueous media are higher. Besides, smaller particle sizes also assist a higher diffusion rate. For these reasons, the rate of DMOG release was higher than that of BSA and their release profiles are different. However, at pH 7.4, the release rate of both DMOG and BSA was higher compared to pH 7.0. Many research groups reported that the release nature of drugs from hydrogels or composite materials is dependent on the rate of swelling of the materials [39, 40]. In this case, the swelling rate of the film was higher at pH 7.4 than at pH 7.0. Consequently, at pH 7.4, the higher rate of water diffusion into the film network induced higher release rates of DMOG and BSA than at pH 7.0.

4. Conclusions

A novel pathway has been designed and applied for the development of a hybrid film (Alg- α -TCP) with excellent characteristics like biocompatibility, mechanical strength, flexibility, and a stimuli-responsive swelling property. Various grades of the hybrid films have been fabricated using alginate as biopolymer, α -TCP as a ceramic and CaCl₂ as a crosslinking agent. A screening technique (like a concrete finishing process) has been applied to get a better orientation of α -TCP micro-particles in the alginate matrix and to achieve flatness in the film. The ATR-FTIR, ¹³C NMR and XRD surface analyses confirmed the ionic crosslinking phenomena and formation of the cross-linked hybrid network. The SEM and FESEM analyses indicated that the α -TCP

micro-particles are orderly distributed into the cross-linked network. TGA analyses implied that the ionic crosslinking as well as the interfacial interaction between alginate and α -TCP enhanced the thermal stability of the hybrid films. The micro-fatigue test result suggested that the mechanical properties of Alg- α -TCP hybrid films depend on the distribution of the ceramic particles (α -TCP) as well as on the composition of the materials. Out of diverse grades of films, Alg- α -TCP (2:1) showed comparatively higher mechanical strength and flexibility. The lower transmission of UV light between 200–250 nm indicates that the Alg- α -TCP film could prevent damage to lipids and medical devices from UV light. The *in vitro* bone cell (MC3T3) culture and cytotoxicity tests showed that the hybrid film is biocompatible. The hybrid film releases two drugs, bovine serum albumin (BSA) and dimethylglycine (DMOG), in a controlled way at pH 7.0 and 7.4, and 37 °C. Finally, the Alg- α -TCP biocompatible film with high mechanical strength and flexibility could be employed as an interfacial film in tissue engineering, such as for osteochondral defects.

Acknowledgments

The authors are thankful to Mr Hoon Choi, Phường Ngân Ngô Đình and Mr Muhamed Mehtab for their cooperation during the work. The authors also sincerely acknowledge the financial support of National Research Foundation of Korea (NRF) Grants (2014K2A2A7060928 and 2015R1A2A1A10054592) and National Natural Science Foundation of China (NSFC No. 81461148032).

ORCID iDs

Insup Noh  <https://orcid.org/0000-0003-0696-7768>

References

- [1] Liao J, Tian T, Shi S, Xie X, Ma Q, Li G and Lin Y 2017 The fabrication of biomimetic biphasic CAN-PAC hydrogel with a seamless interfacial layer applied in osteochondral defect repair *Bone Res.* **5** 17018
- [2] Noeaid P, Salih V, Beier J P and Boccaccini A R 2012 Osteochondral tissue engineering: scaffolds, stem cells and applications *J. Cell. Mol. Med.* **16** 2247–70
- [3] Castro N J, Hacking S A and Zhang L G 2012 Recent progress in interfacial tissue engineering approaches for osteochondral defects *Ann. Biomed. Eng.* **40** 1628–40
- [4] Yang J, Zhang Y S, Yue K and Khademhosseini A 2017 Cell-laden hydrogels for osteochondral and cartilage tissue *Acta Biomater.* **57** 1–25
- [5] Shen T, Dai Y, Li X, Xu S, Gou Z and Gao C 2017 Regeneration of the osteochondral defect by a wollastonite and macroporous fibrin biphasic scaffold *ACS Biomater. Sci. Eng.* (<https://doi.org/10.1021/acsbomaterials.7b00333>)
- [6] Luo Y, Lode A, Sonntag F, Nies B and Gelinsky M 2013 Well-ordered biphasic calcium phosphate–alginate scaffolds fabricated by multi-channel 3D plotting under mild conditions *J. Mater. Chem. B* **1** 4088–98

- [7] Markstedt K, Mantas A, Tournier I, Avila H M, Hagg D and Gatenholm P 2015 3D bioprinting human chondrocytes with nanocellulose-alginate bioink for cartilage tissue engineering applications *Biomacromolecules* **16** 1489–96
- [8] Tritz J et al 2010 Designing a three-dimensional alginate hydrogel by spraying method for cartilage tissue engineering *Soft Matter* **6** 5165–74
- [9] Zeng L, Yao Y, Wang D A and Chen X 2014 Effect of microcavitary alginate hydrogel with different pore sizes on chondrocyte culture for cartilage tissue engineering *Mater. Sci. Eng. C* **34** 168–75
- [10] Jin R, Teixeira L S M, Dijkstra P J, Karperien M, van Blitterswijk C A, Zhong Z Y and Feijen J 2009 Injectable chitosan-based hydrogels for cartilage tissue engineering *Biomaterials* **30** 2544–51
- [11] Choi B, Kim S, Lin B, Wu B M and Lee M 2014 Cartilaginous extracellular matrix-modified chitosan hydrogels for cartilage tissue engineering *ACS Appl. Mater. Interfaces* **6** 20110–21
- [12] Shen Z S, Cui X, Hou R X, Li Q, Deng H X and Fu J 2015 Tough biodegradable chitosan-gelatin hydrogels via *in situ* precipitation for potential cartilage tissue engineering *RSC Adv.* **5** 55640–7
- [13] Luo Y and Shoichet M S 2004 A photolabile hydrogel for guided three-dimensional cell growth and migration *Nat. Mater.* **3** 249–53
- [14] Mauck R L, Yuan X and Tuan R S 2006 Chondrogenic differentiation and functional maturation of bovine mesenchymal stem cells in long-term agarose culture *Osteoarthritis Cartilage* **14** 179–89
- [15] Snyder T N, Madhavan K, Intrator M, Dregalla R C and Park D A 2014 Fibrin/hyaluronic acid hydrogel for the delivery of mesenchymal stem cells and potential for articular cartilage repair *J. Biol. Eng.* **8** 10
- [16] Kim I L, Mauck R L and Burdick J A 2011 Hydrogel design for cartilage tissue engineering: a case study with hyaluronic acid *Biomaterials* **32** 8771–82
- [17] Oliveira J T, Santos T C, Martins L, Picciocchi R, Marques A P, Castro A G, Neves N M, Mano J F and Reis R S 2010 Gellan gum injectable hydrogels for cartilage tissue engineering applications: *in vitro* studies and preliminary *in vivo* evaluation *Tissue Eng. A* **16** 343–53
- [18] Bacelar A H, Correia J S, Oliveira J M and Reis R L 2016 Recent progress in gellan gum hydrogels provided by functionalization strategies *J. Mater. Chem. B* **4** 6164–74
- [19] Han L, Xu J, Lu X, Gan D, Wang Z, Wang K, Zhang H, Yuan H and Weng J 2017 Biohybrid methacrylated gelatin/polyacrylamide hydrogels for cartilage repair *J. Mater. Chem. B* **5** 731–41
- [20] Levingstone T J, Matsiko A, Dickson G R and O'Brien F J 2014 A biomimetic multi-layered collagen-based scaffold for osteochondral repair *Acta Biomater.* **10** 1996–2004
- [21] Miao T, Miller E J, McKenzie C and Oldinski R A 2015 Physically cross-linked polyvinyl alcohol and gelatin interpenetrating polymer network theta-gels for cartilage regeneration *J. Mater. Chem. B* **3** 9242–9
- [22] Dai Y, Liu G, Ma L, Wang D and Gao C 2016 Cell-free macroporous fibrin scaffolds for *in situ* inductive regeneration of full-thickness cartilage defects *J. Mater. Chem. B* **4** 4410–9
- [23] Puppi D, Chiellini F and Piras A M 2010 Polymeric materials for bone and cartilage repair *Prog. Polym. Sci.* **35** 403–40
- [24] Castilho M, Rodrigues J, Pires I, Gouveia B, Pereira M, Moseke C, Groll J, Ewald A and Vorndran E 2015 Fabrication of individual alginate-TCP scaffolds for bone tissue engineering by means of powder printing *Biofabrication* **7** 015004
- [25] Lee G S, Park J H, Shin U S and Kim H W 2011 Direct deposited porous scaffolds of calcium phosphate cement with alginate for drug delivery and bone tissue engineering *Acta Biomater.* **7** 3178–86
- [26] Lee G S, Shin U S, Park J H, Kim H W and Won J E 2011 Alginate combined calcium phosphate cements: mechanical properties and *in vitro* rat bone marrow stromal cell responses *J. Mater. Sci., Mater. Med.* **22** 1257–68
- [27] Perez R A and Kim H W 2013 Core-shell designed scaffolds of alginate/alpha-tricalcium phosphate for the loading and delivery of biological proteins *J. Biomed. Mater. Res. A* **101A** 1103–12
- [28] Perez R A, Kim J H, Buitrago J O, Wall I B and Kim H W 2015 Novel therapeutic core-shell hydrogel scaffolds with sequential delivery of cobalt and bone morphogenetic protein-2 for synergistic bone regeneration *Acta Biomater.* **23** 295–308
- [29] Woo J S and Kim H Y 2012 Effects of dicalcium phosphate on characteristics of alpha tricalcium phosphate and its corresponding calcium phosphate cements *Biomater. Res.* **16** 164–70
- [30] Grant G T, Morris E R, Rees D A, Smith P J C and Thom D 1973 Biological interactions between polysaccharides and divalent cations: the egg-box model *FEBS Lett.* **32** 195–8
- [31] Sikorski P, Mo F, Bræk G S and Stokke B T 2007 Evidence for egg-box-compatible interactions in calcium-alginate gels from fiber x-ray diffraction *Biomacromolecules* **8** 2098–103
- [32] Li L, Fang Y, Vreeker R and Appelqvist I 2007 Reexamining the egg-box model in calcium-alginate gels with x-ray diffraction *Biomacromolecules* **8** 464–8
- [33] Rao A, Quiralta P V, Fernandez M S, Berg J K, Sanchez M, Drechsler M, Carrillo A N, Arias J L, Gebauer D and Colfen H 2016 PH-dependent schemes of calcium carbonate formation in the presence of alginates *Cryst. Growth Des.* **16** 1349–59
- [34] Yang M, Xia Y, Wang Y, Zhao X, Xue Z, Quan F, Geng C and Zhao Z 2016 Preparation and property investigation of crosslinked alginate/silicon dioxide nanocomposite films *J. Appl. Polym. Sci.* **133** 43489
- [35] Jung J P, Bhuiyan D B and Ogle B M 2016 Solid organ fabrication: comparison of decellularization to 3D bioprinting *Biomater. Res.* **20** 27
- [36] Galus S and Lenart A 2013 Development and characterization of composite edible films based on sodium alginate and pectin *J. Food Eng.* **115** 459–65
- [37] Nadagouda M N and Varma R S 2007 Synthesis of thermally stable carboxymethyl cellulose/metal biodegradable nanocomposites for potential biological applications *Biomacromolecules* **8** 2762–7
- [38] Abdollahi M, Alboofetileh M, Behrooz R, Rezaei M and Miraki R 2013 Reducing water sensitivity of alginate bio-nanocomposite film using cellulose nanoparticles *Int. J. Biol. Macromol.* **54** 166–73
- [39] Das R, Das D, Ghosh P, Dhara S, Panda A B and Pal S 2015 Development and application of a nanocomposite derived from crosslinked HPMC and Au nanoparticles for colon targeted drug delivery *RSC Adv.* **5** 27481–90
- [40] Mandal B, Das D, Rameshbabu A P, Dhara S and Pal S 2016 A biodegradable, biocompatible transdermal device derived from carboxymethyl cellulose and multi-walled carbon nanotubes for sustained release of diclofenac sodium *RSC Adv.* **6** 19605–11